A Brillouin scattering study of $La_{0.77}Ca_{0.23}MnO_3$ across the metal–insulator transition

A Brillouin scattering study of $La_{0.77}Ca_{0.23}MnO_3$ across the metal–insulator transition

Md Motin Seikh[1,2]**, Chandrabhas Narayana**[1]**, L Sudheendra**[1]**, A K Sood**[1,3] **and C N R Rao**[1,2]

[1] Chemistry and Physics of Materials Unit, Jawaharlal Nehru Centre for Advanced Scientific Research, Jakkur PO, Bangalore 560 064, India
[2] Solid State and Structural Chemistry Unit, Indian Institute of Science, Bangalore 560 012, India
[3] Department of Physics, Indian Institute of Science, Bangalore 560 012, India

Abstract

Temperature-dependent Brillouin scattering studies have been carried out on $La_{0.77}Ca_{0.23}MnO_3$ across the paramagnetic insulator–ferromagnetic metal (I–M) transition ($T_C \sim 230$ K). The spectra show modes corresponding to a surface Rayleigh wave (SRW) and a high velocity pseudo-surface wave (HVPSAW) along with bulk acoustic waves (B1 and B2). The Brillouin shifts associated with the SRW and HVPSAW increase, whereas the B1 and B2 frequencies decrease, below T_C. The temperature dependence of the SRW and HVPSAW modes is related to the increase in the elastic constant C_{11} across the I–M transition. The decrease in frequency across the I–M transition of the bulk modes is understood to be due to enhanced self-energy corrections as a result of increased magnon–phonon interaction across the I–M transition. Correspondingly, these modes show a large increase in the full width at half maximum (FWHM) as the temperature decreases. We also observe a central peak whose width is maximum at T_C.

1. Introduction

The study of the pervoskite manganites, $A_{1-x}B_xMnO_3$ (ABMO), where A and B are trivalent and divalent ions, respectively, has attracted much attention due to their fascinating properties and technological potential [1]. In particular, $La_{0.77}Ca_{0.23}MnO_3$ (LCMO) composite exhibits a transition from a paramagnetic insulating to a ferromagnetic metallic state for $0.2 \leqslant x \leqslant 0.5$ and shows colossal magnetoresistance. In ABMO type manganites, the transition temperature as well as other properties are markedly affected by the average radius of the A-site cations, and in turn affect the band width of the e_g electrons due to the Mn^{3+} ions. Jahn–Teller based electron–phonon coupling [2, 3] as well as the double exchange [4] play important roles in determining the properties of the manganites. There is experimental evidence for the presence

of lattice distortions [5–8] which give rise to polarons which may have a lattice type and/or magnetic origin [9, 10].

Brillouin scattering is a powerful probe to study the surface and bulk acoustic phonons as well as magnetic excitations in opaque solids [11]. The surface phonon can give rise to a surface Rayleigh wave (SRW), a pseudo-surface acoustic wave (PSAW) and a high velocity pseudo-surface acoustic wave (HVPSAW) [12]. The pointing vector of the SRW lies parallel to the free surface and its particle displacement field decays exponentially within the medium. On the other hand, both the PSAW and the HVPSAW radiate energy into the bulk and are attenuated due to their decay into the bulk phonons. Unlike the SRW, the PSAW propagates only along some specific directions of the anisotropic medium and its phase velocity is ~40% higher than the SRW velocities [13–15]. In comparison, the HVPSAW propagates in both anisotropic as well as isotropic media [16] and has a phase velocity nearly twice that of the regular SRW [13–15]. The PSAW and HVPSAW modes can have potential applications in surface acoustic wave devices due to their higher frequencies relative to the SRW [13–15].

We have carried out a Brillouin scattering investigation of LCMO, which exhibits the paramagnetic insulator–ferromagnetic metal (I–M) transition at a T_C of 230 K. In addition to the SRW, the HVPSAW mode is also observed in this system. A similar observation has been made in our earlier work on $Nd_{0.5}Sr_{0.5}MnO_3$ [17]. The SRW and HVPSAW mode frequencies increase whereas the frequency of the bulk phonon decreases below T_C. The temperature dependence of both the surface modes can be understood in terms of the temperature dependence of the elastic constants. Along with the surface acoustic modes, we also observe bulk acoustic modes (BAWs). The softening of these modes, along with an increase in their width with the decrease in temperature, is suggested to arise from an increase in the self-energy contribution associated with the magnon–phonon interaction across the I–M transition. A central peak is also observed and its width becomes maximum at T_C.

2. Experimental details

Polycrystalline powder of LCMO was prepared by the solid-state reaction of stoichiometric amounts of lanthanum acetate, calcium carbonate and manganese dioxide. The materials were ground and heated at 1000 °C for 60 h with two intermediate grindings. The sample was then further heated at 1200 °C for 48 h. The polycrystalline powder was placed in a latex tube and pressed using a hydrostatic pressure of 5 tons. The rods thus obtained were sintered at 1400 °C for 24 h. The rods were then used to grow crystals by the floating zone melting technique. The technique employs an SC-M35HD double-reflector image furnace (Nichiden Machinery Ltd, Japan). The growth rate and rotation speed were 10 mm h^{-1} and 30 rpm, respectively. The composition of the crystal was determined using energy dispersive analysis of x-rays (EDAX) using a LEICA S440I scanning electron microscope (SEM) from M/s LEICA, Japan, using a Si–Li detector. The percentage of the Mn^{4+} was determined to be 23 ± 2%.

Brillouin spectra were recorded in the back-scattering geometry with an incident angle $\theta = 45°$ with respect to the surface normal using a JRS Scientific Instruments 3 + 3 pass tandem Febry–Perot interferometer equipped with a photo-avalanche diode as a detector. We would like to mention here that the temperature-dependent experiments were carried out on the B1-mode in the 90° scattering geometry to avoid the strong reflection artifact peaks, which can appear around 27 and 33 GHz in the back-scattering geometry. The Nd:YAG single-mode solid-state diode-pumped frequency doubled laser (DPSS 532–400, Coherent Inc., USA) operating at 532 nm and a power of ~25 mW (focused to a diameter of ~30 μm) was used to excite the spectra. The temperature experiments were carried out using a closed cycle helium cryostat (CTI Cryogenics, USA). The sample temperature was measured with an accuracy of
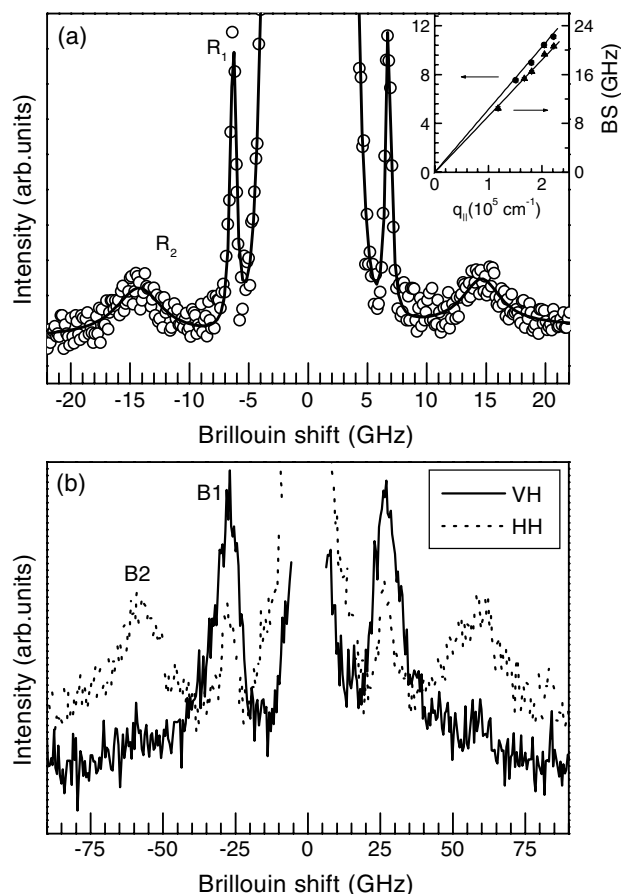
Figure 1. The room temperature Brillouin spectra of La$_{0.77}$Ca$_{0.23}$MnO$_3$. (a) Both the surface acoustic modes SRW and HVPSAW assigned as R$_1$ and R$_2$, respectively. The inset shows their linear dependence on $q_\parallel$ (circle and uptriangle for SRW and HVPSAW, respectively). (b) Polarization dependence of the bulk acoustic modes, B1 and B2. The B2 mode appears only in parallel polarization (HH) (dotted spectrum), whereas the B1 mode appears in both cross (VH) and parallel (HH) polarization with different intensities (see the text for discussion).

±1 K. There is no laser damage of the sample surface as verified under a high magnification microscope. The typical time required per spectrum was 1.5 h. The laser-induced heating of the sample is estimated to be 66 K, as measured from the anti-Stokes to Stokes intensity ratio of the 480 cm^{-1} Raman band of the sample recorded under similar experimental conditions. The data presented here have been corrected to take the laser heating into account.

3. Results and discussion

Figure 1 shows the Brillouin spectra recorded using two spectral ranges at room temperature outside the cryostat. The spectra reveal four modes: 6.8 GHz (labelled as R$_1$), 15.3 GHz (R$_2$), 24 GHz (B1) and 58 GHz (B2). The inset in figure 1(a) shows the linear dependence of the R$_1$ and R$_2$ mode frequencies as a function of magnitude of the wavevector parallel to the surface, $q_\parallel$, thereby establishing them to be the surface modes. Upon rotating the crystal about the normal to the surface, the R$_1$ mode frequency shows an oscillatory behaviour as a function of the rotation angle ϕ, as expected of an SRW. The R$_2$ mode is associated with the HVPSAW since its frequency is almost double that of the R$_1$ mode, with a much broader line-width. A similar mode observed in GaAs along (1$\bar{1}$1) has been discussed in the literature [12–15]. In addition, a weak but sharp peak occurs at 8.6 GHz. This mode appears at certain orientation of the crystal and its frequency also shows a linear dependence on $q_\parallel$, suggesting this to be the PSAW mode. The PSAW and HVPSAW modes appear in the spectra because the sample

surface is not along any specific crystallographic direction. The peaks labelled B1 and B2 in figure 1 are associated with the bulk acoustic waves. The line-widths of these modes are much higher due to the uncertainly in the wavevector arising from the finite penetration depth, δ, of the incident radiation.

The polarization dependence of the B1 and B2 modes at room temperature is shown in figure 1(b). The B2 mode appears only when the incident and scattering polarizations are horizontal (H), i.e. in the scattering plane or s polarized, suggesting thereby that it is a longitudinal acoustic (LA) mode. On the other hand, the B1 mode becomes strong when the incident polarization is vertical (V), i.e. perpendicular to the scattered plane or p polarized, and the scattered light is H polarized (s polarized). When both the incident and the scattered polarization are H polarized, the B1 mode is rendered weaker, with the full width at half maximum (FWHM) becoming nearly half of the value in the VH configuration.

The temperature dependence of the frequencies of the different modes of LCMO is presented in figure 2, where $\Delta\omega = \omega(T) - \omega(370 \text{ K})$. We see from figure 2(a) that the frequency of the SRW (R_1) mode increases below T_C. There is a gradual increase in the HVPSAW mode frequency as the temperature is lowered (see figure 2(b)). The B1 and B2 modes, on the other hand, show a downward jump in frequency at T_C as can be seen from figures 2(c) and (d) respectively. The inset in figure 2(c) displays the magnetic field (H) dependence of the B1 mode frequency at room temperature showing an increase of about 8% with the magnetic field of only 0.35 T. This observation suggests that the B1 mode has strong coupling to magnetic excitations. The B2 mode does not show any dependence on H. The anomalous temperature-dependent behaviour of FWHM of the B1 and the B2 modes is shown in figure 3. The FWHM increases with the decrease in temperature, because the uncertainty in the wavevector due to finite penetration depth of light is proportional to the square root of the conductivity, which increases with the decrease in temperature (as shown in the inset of figure 3). This broadening makes the observation of these modes difficult below $\sim$150 K.

We now discuss the temperature dependence of the various modes. The SRW frequency can be calculated using the Green function method [18, 19], which requires the values of the elastic constants and mass density. Since the orthorhombic distortions in LCMO are not large, we can assume it to be cubic and use the three elastic constants C_{11}, C_{12} and C_{44} to calculate the SRW frequency. Unfortunately, the elastic constants of LCMO are not available in the literature and we have, therefore, used the experimental values of elastic constants of $La_{0.835}Sr_{0.165}MnO_3$ (LSMO) [20], measured as a function of temperature using ultrasound attenuation. This has been reproduced in figure 4(a). Since the LCMO crystal was not cut along any direction, we are not able to use any known elastic modulus equations to fit the data. The present discussion is, therefore, qualitative. The Green function method used here to calculate the SRW frequency of LSMO is for the (100) surface. The elastic constants values of LCMO should be similar to those of LSMO, since the calculated SRW mode frequency for LSMO for $\theta = 45°$ matches the observed data of LCMO at 300 K. Figure 4(b) shows the calculated SRW for LSMO and the experimentally obtained SRW of LCMO. The hardening in the velocities below T_C in both these manganites is similar. In LSMO, the hardening of the bulk sound velocity is observed, for $0.11 \leqslant x \leqslant 0.17$, below T_C [21]. A 5% hardening in the bulk sound velocity is found in the case of $La_{0.67}Ca_{0.33}MnO_3$ below T_C [22]. The origin of the hardening of the sound velocity below T_C should be the same in all these materials exhibiting an I–M transition. It is suggested [23] that the sound velocity increases below T_C due to the decrease in the electron–phonon coupling arising from the high mobility of carrier in the metallic state. Application of an external magnetic field increases the sound velocity, since the magnetic field greatly enhances the mobility of the carriers [23]. In the high temperature insulating phase, the electron–phonon coupling is large, giving rise to a smaller frequency of the acoustic phonon.
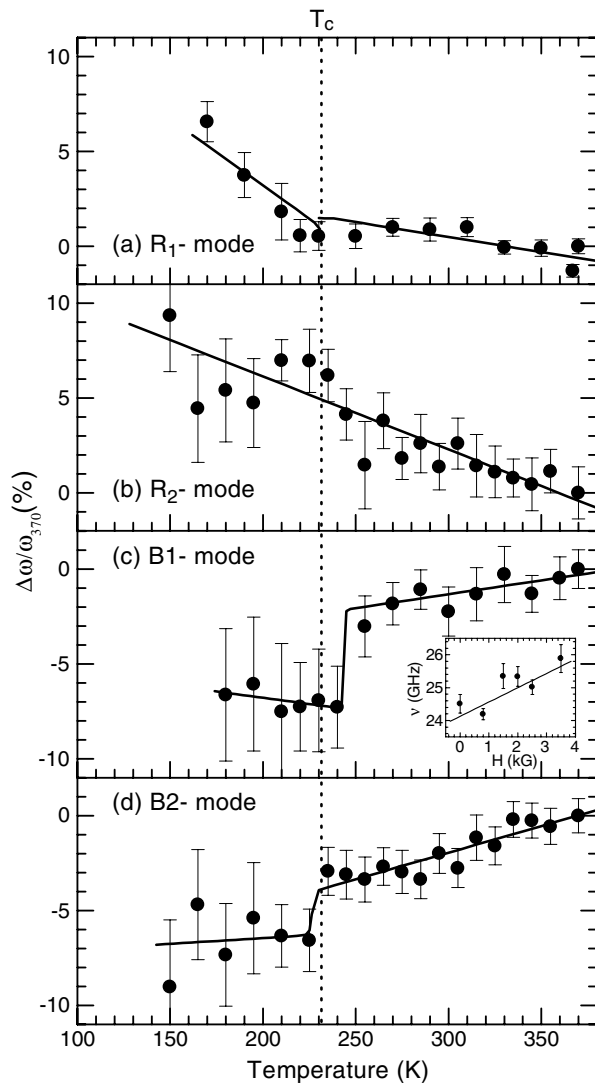
Figure 2. The temperature dependence of the changes in frequencies of all the four modes. (a), (b) The hardening of the surface modes SRW and HVPSAW, respectively. (c), (d) The softening of the B1 and B2 modes, respectively. The inset of (c) shows the variation in the frequency of the B1 mode with the applied magnetic field at room temperature.

The temperature dependence of the HVPSAW mode frequency also arises due to the increase in C_{11} and C_{44} across the I–M transition, just as in the case of the SRW mode.

A ~3% softening of the B1 and B2 modes is observed across the I–M transition temperature (see figures 2(c) and (d)). The change in the Brillouin shift associated with the bulk acoustic mode ($\omega = vq$, where v is the sound velocity) has two contributions, that is, $\Delta\omega/\omega = \Delta v/v + \Delta n/n$; where the second term arises from the change in wavevector q due to the change in the refractive index, n, of the material. Ultrasonic measurements have shown that the sound velocity increases in the metallic phase by $\Delta v/v = +3\%$ [24]. A change of -3% in $\Delta\omega/\omega$ requires a change of $\Delta n/n = -6\%$. Since there are no measurements of refractive index as a function of temperature in manganites, we are unable to decide whether the observed change in ω is entirely due to change in the refractive index. If the observed decrease in the Brillouin shift is not explained by a decrease in n, one has to think of mechanisms in terms of coupling of the acoustic mode with electronic and spin excitations.
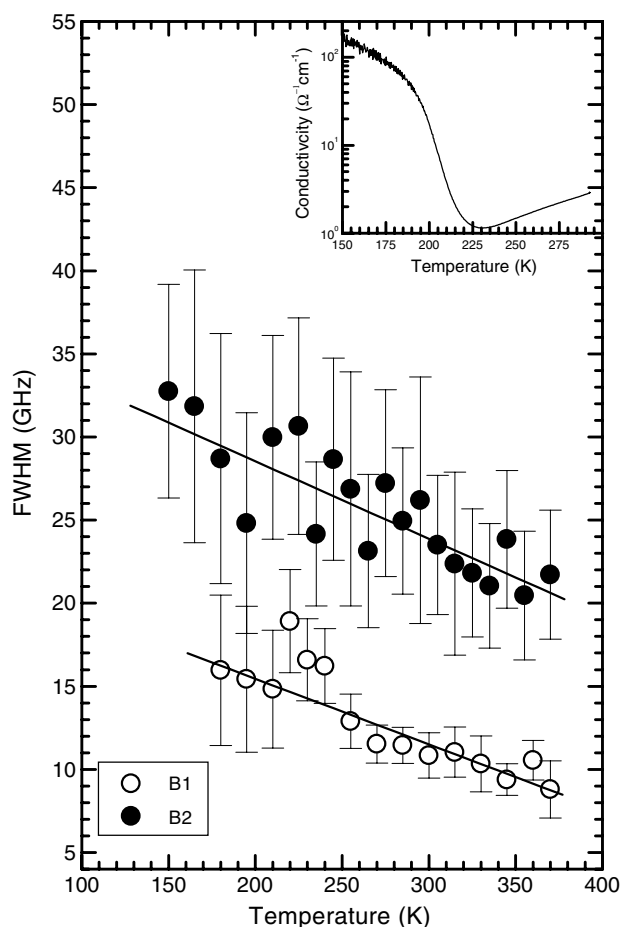
Figure 3. Variation of the line-width as a function of temperature for both B1 (open circle) and B2 (solid circle) modes. The inset shows the conductivity data of the sample on which Brillouin studies were carried out.

In figure 5, we show the Brillouin spectra of LCMO in the 90° scattering geometry at various temperatures, revealing the presence of a central mode between 290 and 180 K. We used three Lorentzian functions with an appropriate background, to fit the spectrum at each temperature. For temperatures below 180 K and above 290 K, we obtain a perfect fit with the elastically scattered mode having a FWHM mode of 0.6 GHz over the entire 150–370 K range. Between 290 and 180 K, it was difficult to fit the spectra in this manner. Taking the FWHM of the elastically scattered mode as 0.6 GHz and adding an additional Lorentzian centre at $\omega = 0$, a good fit could be obtained as shown in (c) and (d) of figure 5. This fit gives the temperature dependence of the FWHM of the central mode. The temperature dependence of the intensity is similar, showing that the width and intensity are maximum near T_C. A similar observation of the central peak has been made in neutron scattering experiments across the paramagnetic to ferromagnetic transition [25–29], but at a much larger value of $q \sim 0.1$–0.3 Å^{-1} in $La_{1-x}Ca_xMnO_3$ ($x = 0.2, 0.25, 0.3$ and 0.33), $Nd_{0.7}Sr_{0.3}MnO_3$ and $Pr_{0.63}Sr_{0.37}MnO_3$. The presence of the central peak in the manganite suggests the existence of competing magnetic states. In the neutron diffraction measurements [29], the spectral weight of the spin-wave excitation decreases as $T \rightarrow T_C$, while the weight for the spin-diffusion component increases rapidly. The spin-diffusion component dominates the fluctuation spectrum near T_C, in marked contrast to conventional ferromagnets. If one assumes spin diffusion as the origin of the central
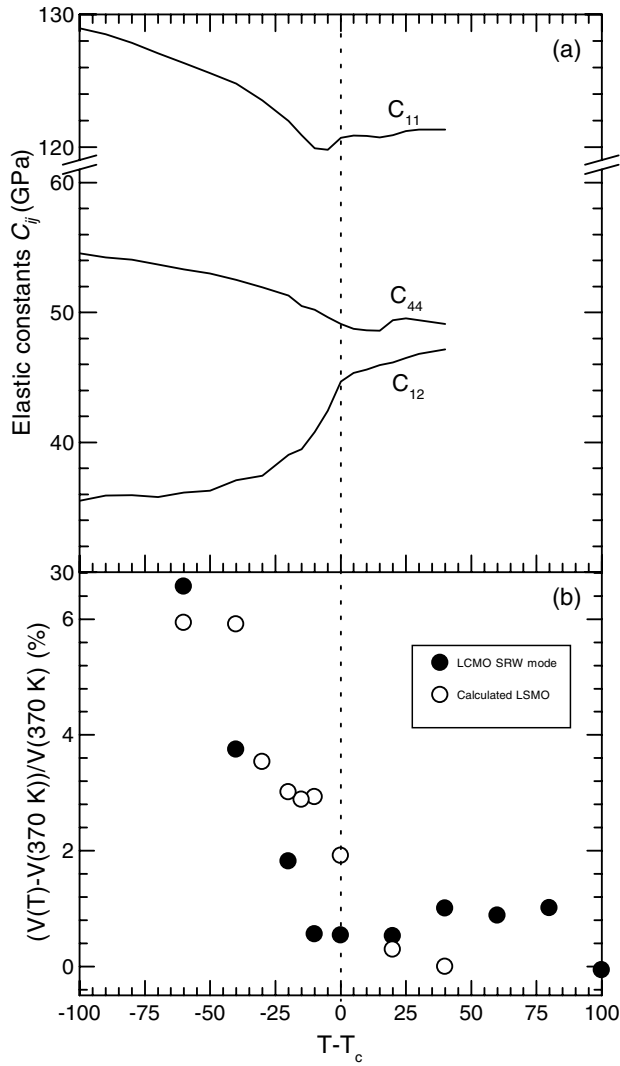
Figure 4. (a) The temperature dependent elastic constants of $La_{0.835}Sr_{0.165}MnO_3$ (LSMO) taken from [20]. (b) Relative changes in the surface sound velocity with temperature: calculated sound velocity along (100) direction (open circle) for LSMO using the elastic constants data presented in panel (a) and our experimental data of LCMO (solid circle).

peak in the present study, then the intrinsic width (FWHM or Γ_c) of the central peak is given by $\Gamma_c = \Lambda q^2$, where Λ is the spin diffusivity. In the present study, $\Gamma/2\pi = 21$ GHz at T_C (see figure 6) and $q = 3.675 \times 10^{-3}$ Å^{-1} leading to the value of spin diffusivity Λ of 40.4 eV Å^{-2}, a value which is much larger than that observed in the case of $Nd_{1-x}Sr_xMnO_3$ ($x = 0.3$), where $\Lambda = 26(2)$ meV Å^{-2} [29]. Thus, the origin of the central peak in the present case does not appear to be spin diffusion.

Entropy fluctuations with a width $\Gamma_S = 2Kq^2$ [30, 31], where K is the thermal diffusivity ($K = \kappa/C\rho$, where κ is the thermal conductivity, C is the specific heat and ρ is the density of the medium), can also be the origin of the quasielastic scattering. The value of κ at 300 K is 22.9 mW cm^{-1} K^{-1} (for LCMO ($x = 0.25$)) [32], while $C = 75.5$ J mol^{-1} K^{-1} and $\rho = 6.2$ g cm^{-3} giving $\kappa = 1.1 \times 10^{-2}$ cm^2 s^{-1}. The width Γ turns out to be 3 GHz. Taking $\rho(T)$, $C(T)$ and $\kappa(T)$ for LCMO ($x = 0.25$), the temperature dependence of Γ is obtained as shown in the inset of figure 6. The temperature dependence of Γ_S is in contrast to that observed in figure 6, showing that entropy fluctuations are not responsible for the central mode.
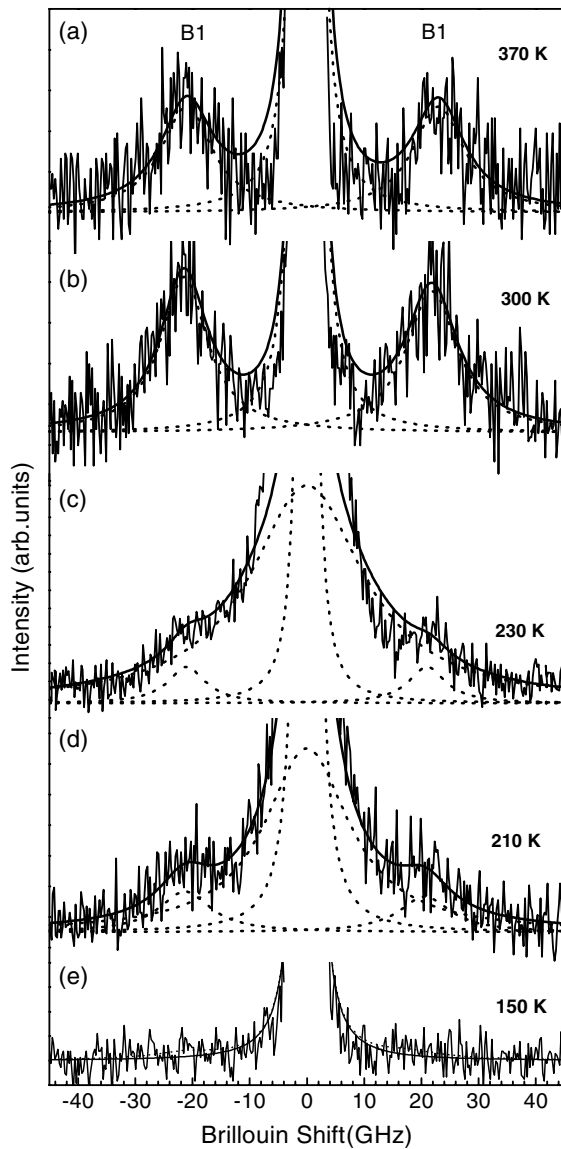
Figure 5. Typical spectrum recorded at different temperatures with 90° scattering geometry, showing the evolution of the central peak in the neighbourhood of T_C (230 K), followed by its disappearance below T_C and also softening of the B1 mode with the decrease in temperature. Dotted curves are the deconvoluted spectra.

Entropy fluctuation can also be viewed as fluctuation in the density of the phonon q_1, which scatters light by the two-phonon difference process involving emission of a phonon q_1 with simultaneous absorption of a phonon $q_1 - q$ from the same branch [30]. In the microscopic picture, scattering of light describes either the indirect [33] or direct [34] coupling of light to phonon density fluctuations, assuming at all times local thermodynamic equilibrium. Along with these, there is also the contribution to phonon density fluctuations from additional dielectric fluctuations, away from the local thermodynamic equilibrium [35]. In this case, the two-phonon difference process is dominated by zone boundary phonons where the density of states is high, leading to the broad central peak extending beyond the Brillouin peaks. The line-width of such a central peak is independent of q [30]. The central peak will, therefore, have a narrow component with line-width of κq^2 and a q-independent broad component from
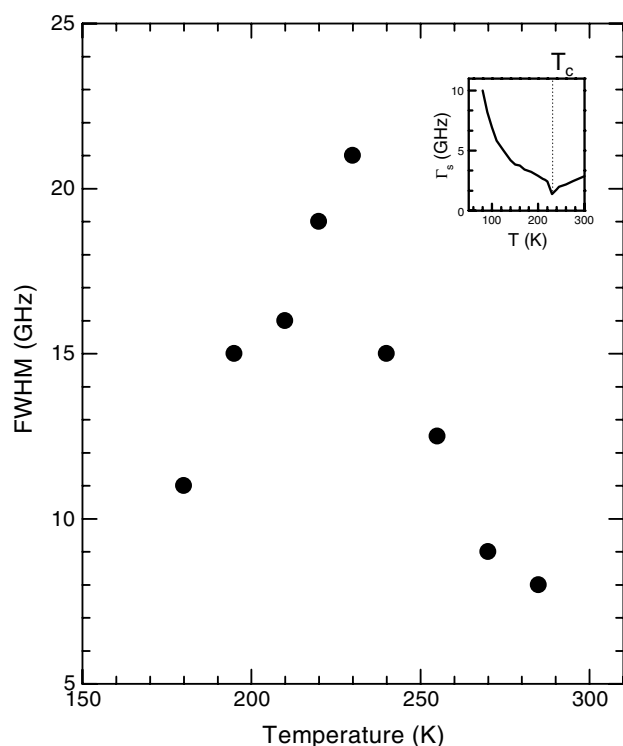
Figure 6. Temperature-dependent line-width of the central peak showing maximum value at T_C. The inset shows the calculated line-width as a function of temperature of the central peak (assuming the entropy fluctuations as the origin) for LCMO ($x = 0.25$) (see text for detailed discussion).

dielectric fluctuations. Since the central mode in our experiments, shown in figure 5, extends right up to the bulk modes, we suggest that it is associated with the q-independent dielectric fluctuations. It has been proposed that defects can contribute to the central peak [36]. In the present case, the defect can be the ferromagnetic insulating phase present before the I–M transition in LCMO [37].

In conclusion, Brillouin scattering experiments on LCMO reveal the presence of a high-velocity pseudo-surface acoustic wave in manganites. The hardening of the SRW frequency below T_C arises from the temperature dependence of C_{11} and C_{44}. The central peak is suggested to arise from non-equilibrium dielectric fluctuations linked to the presence of a ferromagnetic insulating phase preceding the I–M transition. We trust that the present experiments will motivate theoretical studies to quantitatively understand the origin of the central mode and coupling of the acoustic mode with other excitations.

Acknowledgments

References

[1] Jin S, Tiefel T H, McCormack M, Fastnacht R A, Ramesh R and Chen L H 1994 *Science* **264** 413
    Rao C N R and Raveau B (ed) 1998 *Colossal Magnetoresistance, Charge-Ordering and Related Properties of Manganese Oxide* (Singapore: World Scientific)

[2] Millis A J and Shraiman B I 1996 *Phys. Rev. Lett.* **77** 175
     Mahesh R, Mahendiran R, Raychoudhuri A K and Rao C N R 1995 *J. Solid State Chem.* **114** 297
[3] Roder H, Zang J and Bishop A R 1996 *Phys. Rev. Lett.* **76** 1356
[4] Zener C 1951 *Phys. Rev.* **82** 403
     Gennes P G 1960 *Phys. Rev.* **118** 141
[5] Dai P, Zhang J, Mook H A, Liou S-H, Dowben P A and Plummer E W 1996 *Phys. Rev.* B **54** R3694
[6] Billinge S J L, DiFrancesco R G, Kwei G H, Neumeier J J and Thompson J D 1996 *Phys. Rev. Lett.* **77** 715
[7] Radaelli P G, Marezio M, Hwang H Y, Cheong S-W and Batlogg B 1996 *Phys. Rev.* B **54** 8992
[8] Zhao G-M, Conder K, Keller H and Muller K A 1996 *Nature* **381** 676
[9] de Teresa J M, Ibarra M R, Algarabel P A, Ritter C, Marquina C, Blasco J, Garcia J, del Moral A and Arnold Z 1997
     Nature **386** 256
[10] Erwin R W, Lynn J W, Borchers J A, Peng J L and Greene R L 1996 *J. Appl. Phys.* **81** 5487
[11] Murugavel P, Narayana C, Raju A R, Sood A K and Rao C N R 2000 *Europhys. Lett.* **52** 461
[12] Carlotti G, Fioretto D, Giovannini L, Nizzoli F, Socino G and Verdini L 1992 *J. Phys.: Condens. Matter* **4** 257
[13] da Cunha M P and Adler E L 1995 *IEEE Trans. Ultrason. Ferroelectr. Freq. Control* **42** 840
[14] da Cunha M P 1998 *IEEE Trans. Ultrason. Ferroelectr. Freq. Control* **45** 604
[15] da Cunha M P 2001 *Advances in SAW Technology, Systems and Application* vol 2, ed C W Ruppel and
     T A Fjeldly (Singapore: World Scientific) pp 203–43
[16] Camley R E and Nizzoli F 1995 *J. Phys.: Condens. Matter* **18** 4795
[17] Seikh Md M, Narayana C, Parashar S and Sood A K 2003 *Solid State Commun.* **127** 209
[18] Comins J D 2001 *Handbook of Elastic Properties in Solid, Liquids and Gases, Dynamical Methods for Measuring
     the Elastic Properties of Solids* vol 1, ed A G Every and W Sachse (New York: Academic) p 349
[19] Zhang X, Comins J D, Every A G, Stoddart P R, Pang W and Derry T E 1998 *Phys. Rev.* B **58** 13677
[20] Hazama H, Nemoto Y, Goto T, Asamitsu A and Tokura Y 2000 *Physica* B **281/282** 487
[21] Fujishiro H, Ikebe M, Konno Y and Fukase T 1997 *J. Phys. Soc. Japan* **66** 3703
[22] Ramirez A P, Schiffer P, Cheong S-W, Chen C H, Bao W, Palstra T T M, Gammel P L, Bishop J D and
     Zegarski B 1996 *Phys. Rev. Lett.* **76** 3188
[23] Lee J D and Min B I 1997 *Phys. Rev.* B **55** 12454
[24] Zheng R K, Zhu C F, Xie J D, Huang R X and Li X G 2002 *Mater. Chem. Phys.* **75** 121
[25] Lynn J W, Erwin R W, Borchers J A, Huang Q, Santoro A, Peng J L and Li Z Y 1996 *Phys. Rev. Lett.* **76** 4046
[26] Dai P, Hwang H Y, Zhang J, Fernandez-Baca J A, Cheong S-W, Kloc C, Tomioka Y and Tokura Y 2000 *Phys.
     Rev.* B **61** 9553
[27] Dai P, Fernandez-Baca J A, Plummer E W, Tomioka Y and Tokura Y 2001 *Phys. Rev.* B **64** 224429
[28] Besuker G I 1990 *Phys. Status Solidi* b **162** K123
     Jiang F M and Kojima S 2000 *Phys. Rev.* B **62** 8572
[29] Fernandez-Baca J A, Dai P, Hwang H Y, Kloc C and Cheong S-W 1998 *Phys. Rev. Lett.* **80** 4012
[30] Sandercock J R 1982 *Light Scattering in Solids* vol 3, ed M Cardona and G Guntherodt (Berlin: Singapore)
     p 173
[31] Fabelinskii I L 1994 *Phys.—Usp.* **37** 821
[32] Fujishiro H and Ikebe M 2001 *Heat Transport Anomalies around Ferromagnetic and Charge-Order Transitions in
     $La_{1-x}Ca_xMnO_3$, Physics in Local Lattice Distortions* ed H Oyanagi and A Bianconi (New York: American
     Institute of Physics) p 433 (figure 4(a))
     (http://ikebehp.mat.iwate-u.ac.jp/ECMR.html)
[33] Landau L D and Placzek G 1934 *Phys. Z. Sow.* **5** 172
[34] Wehner R K and Klein R 1972 *Physica (Utrecht)* **62** 161
[35] Coombs G J and Cowley R A 1973 *J. Phys. C: Solid State Phys.* **6** 121
[36] Schwabl F and Tauber U C 1991 *Phys. Rev.* B **43** 11112
[37] Huang Q, Lynn J W, Erwin R W, Santoro A, Dender D C, Smolyaninova V N, Ghosh K and Greene R L 2000
     Phys. Rev. B **61** 8895